Supplementary information

Membrane potential drives direct translocation of cell-penetrating peptides

Xinli Gao,[a] Song Hong,[a] Zhiping Liu,[a] Tongtao Yue,[b] Jure Dobnikar[cde] and Xianren Zhang[a]

[a] *State Key Laboratory of Organic-Inorganic Composites, Beijing University of Chemical Technology, Beijing 100029, China*

[b] *State Key Laboratory of Heavy Oil Processing, College of Chemical Engineering, China University of Petroleum (East China), Qingdao 266580, China*

[c] *Beijing national laboratory for condensed matter physics & CAS key laboratory of soft matter physics, Institute of physics, Chinese Academy of Sciences, Beijing 100190, China*

[d] *School of physical sciences, University of Chinese Academy of Sciences, Beijing 100049, China*

[e] *Department of Chemistry, University of Cambridge, Lensfield Road, CB21EW Cambridge, UK.*

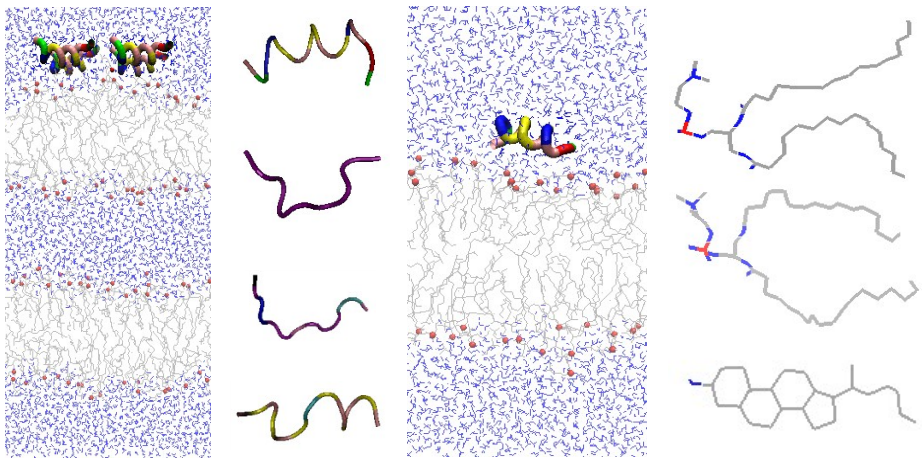

(a) (b) (c) (d)

Fig. S1 Simulation models and system setup. (a) Two-bilayer model with four peptides positioned above the upper lipid bilayer. (b) The models of four different peptides including INLK, R9, TAT and WALP from top to down. (c) One-bilayer model with one peptide positioned above the membrane. (d) DPPC, POPC, and cholesterol molecules used in our simulations.

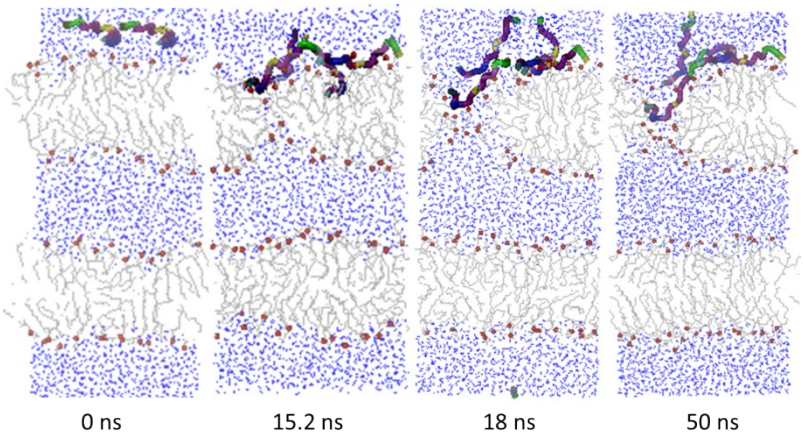

Fig. S2 Time sequence of typical snapshots depicting membrane poration and translocation of four TAT peptides with the membrane potential induced by five pairs of ionic imbalance.

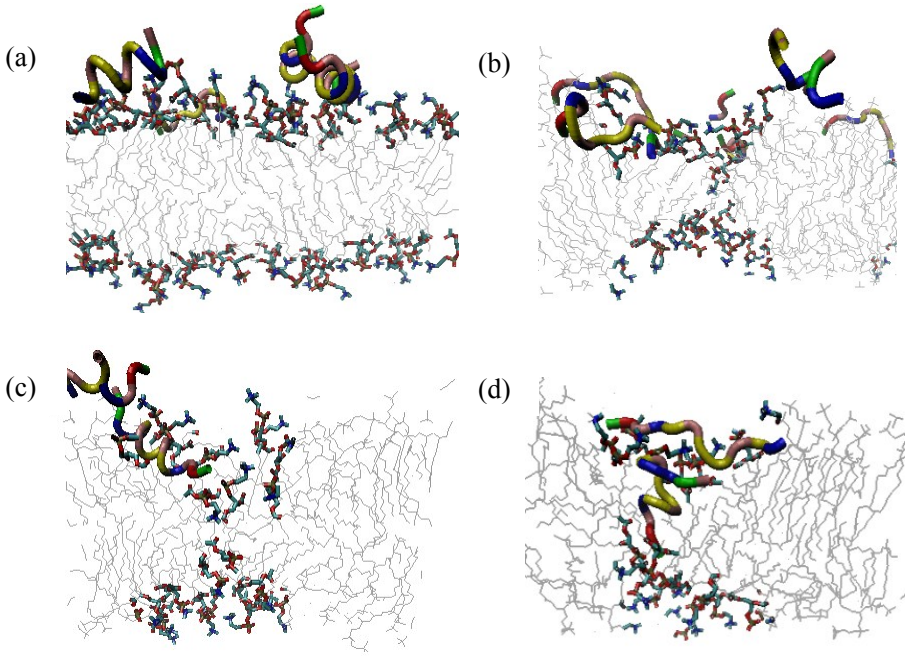

Fig. S3 Locally enlarged configurations showing detailed membrane structural change during interaction with INLK peptides. The membrane potential is produced by three pairs of ionic imbalance.

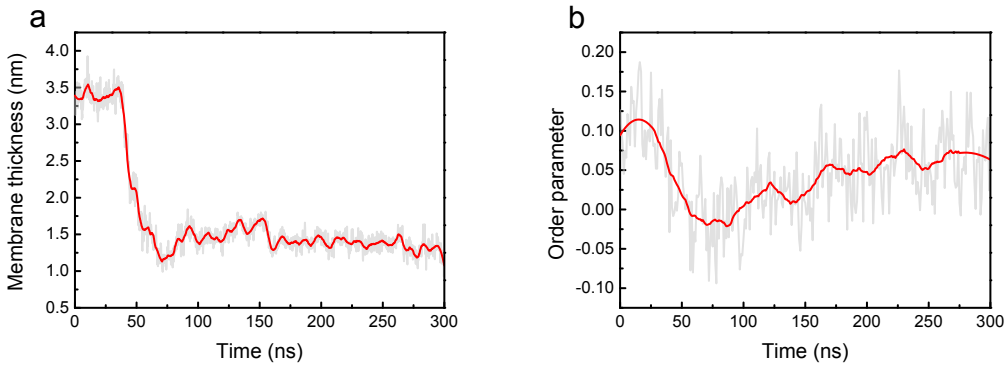

Fig. S4 Time evolutions of both the local membrane thickness (a) and average lipid order parameter around the pore (b).

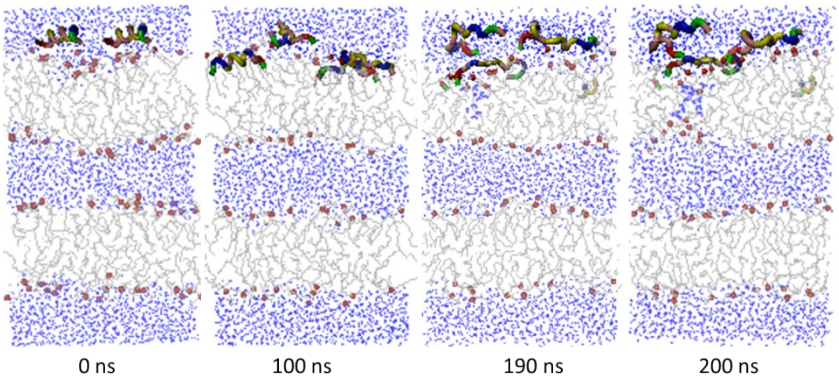

Fig. S5 Time sequence of typical snapshots showing the slow pore formation in POPC bilayer with four ILNK peptides. The transmembrane potential is produced by five pairs of ionic imbalance.

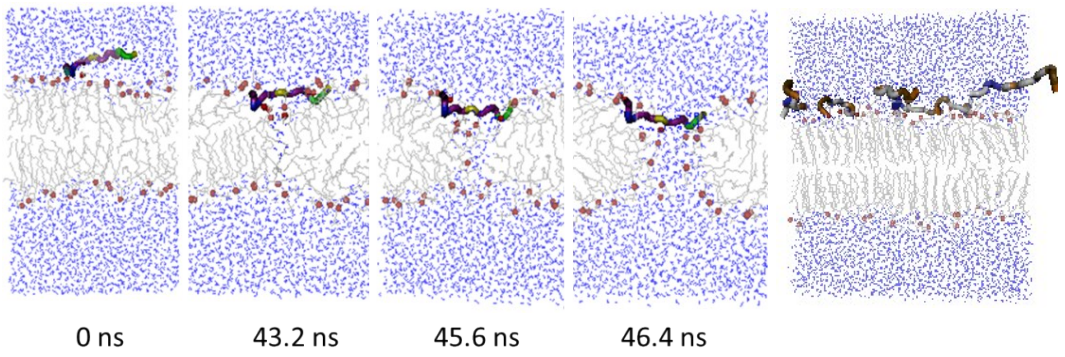

(a) (b)

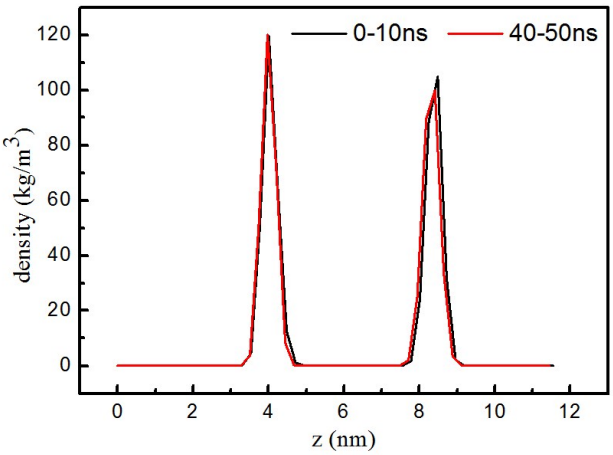

(c)

Fig. S6 The effect of cholesterol on translocation of peptides across the membrane in the presence of an external electric field of 0.18 V/nm. (a) Time sequence of typical snapshots showing poration of the membrane in the absence of cholesterol. (b) The final snapshot after 100 ns simulation showing failed translocation of ILNK peptides across the membrane containing 64 cholesterol molecules. (c) The density distributions of phosphorus atoms of the system containing 64 cholesterols along z direction averaged from two stages of the simulation.

Note 1: The translocation process of INLK

Fig. 2 shows several typical snapshots during the translocation process of INLK peptides. At ~10 ns of the early stage, the floating cell-penetrating peptides in water environment approached the bilayer membrane. Because of the attraction between positively charged lysine (LYS4) residues of INLK and the head groups $PO4^-$ of phospholipid molecules, peptides moved to contact with the membrane. As the simulation proceeded, the INLK peptides partially inserted into the membrane, and their interaction with phospholipid molecules reduced locally the membrane thickness. At 41.6 ns, a number of water molecules run into the lipid membrane and finally, a hydrophilic pore forms at 44 ns. On the other hand, the leucine (Leu14) residues and the isoleucine (Ile1) residues of the INLK peptide are hydrophobic, and thus they prefer to stay within the hydrophobic core of the lipid membrane. Therefore, the peptide touched with the hydrophobic acyl chains of phospholipid molecules, and eventually the hole became nearly hydrophobic with embeded peptides inside. After some hydrophilic residues finally reaches another leaflet of the membrane, and peptide translocation is achieved.

In the process of pore formation and CPP penetration, the positions of nearby phospholipid molecules also change accordingly. By calculating the trajectory of some representative phosphorus atoms on phospholipid head groups, we find that the lipid molecules nearby the pore fluctuate sharply during the processes, as shown in Fig. S7a. Before 44 ns, the fluctuation of different phosphorus atoms keeps in a stable level. However, as the membrane pore began to appears (at about ~44 ns, see Fig. 2), one head group belonging to a lipid molecule in the upper leaflet (denoted as P(#194)) changed its position along z direction sharply and moves to pore center. At the same time, the head group of another lipid (denoted as P(#155) in Fig. S7a) in the lower leaflet went up and moved to the upper leaflet. Besides, some of lipid molecules were found to flip and then went back to the original leaflet (see, e.g., P(#239) in Fig. S7a). This observation suggests that the phospholipid molecules near the pore fluctuate strongly as the pore forms, and also verifies the transformation from hydrophobic hole to hydrophilic hole as CPP penetrates.

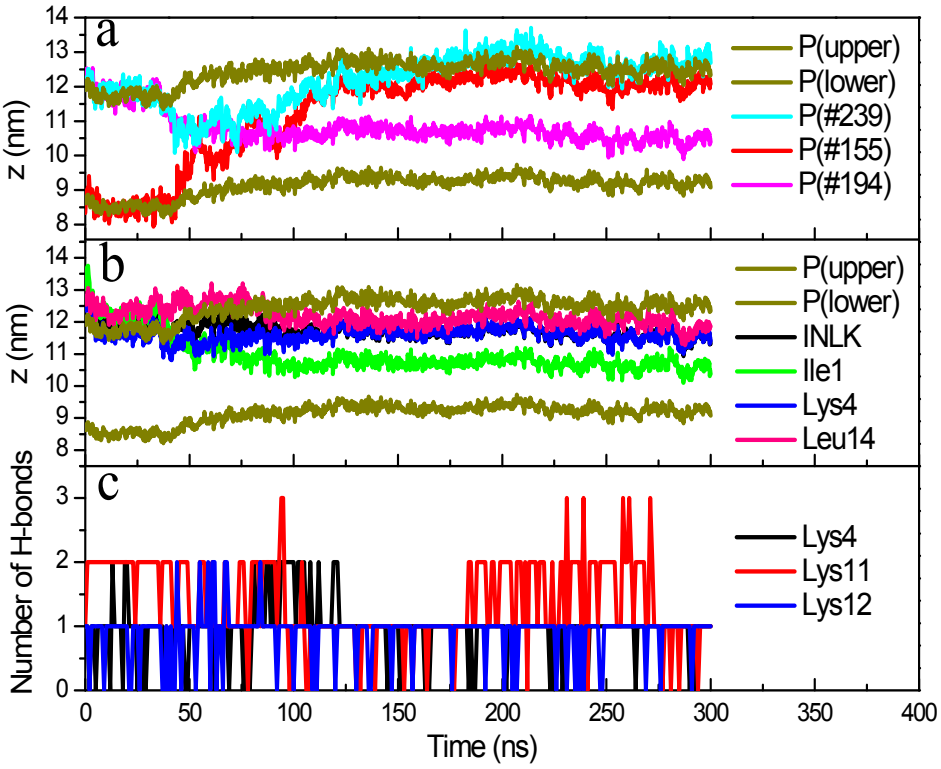

Fig. S7 The dynamics for water pore formation and CPP translocations. (a) The head positions for several phospholipids change as a function of the simulation time from 0ns to 300ns. One phosphate group initially belonging to a lipid molecules in the lower leaflet (denoted as P(#155)) is shown in the figure. While two phosphate groups in the upper leaflet (P(#194) and P(#239)) corresponds to a position nearby the membrane pore. (b) The position of the peptide chain and its residues. (c) The number of hydrogen bonds formed by Lys4, Lys11 and Lys12 with lipid phosphate groups. The average head positions for the upper and lower leaflets (denoted as upper and lower respectively) are shown for comparison.

As described above, when the structure of water hole through the bilayer membrane becomes stable, the peptides begin to move into the membrane along the pore direction (Fig. S7a). We also give the trajectory of the INLK peptide as well as those for its residues. As shown in Fig. S7b, the whole peptide (black line) and different residues kept their positions before 44 ns, and then the peptide began to move down along z direction at ~ 50 ns. The isoleucine (Ile1), which is located at one end of the amino acid sequence and of the hydrophobic nature, moved to the center of the bilayer first, followed by the hydrophilic lysine (Lys4). At this time, other residues

were still in the water environment. As the simulation run proceeded, the residues inserted into the membrane sequentially. The penetration process is achieved as the last residue, the leucine (Leu14), entered the membrane. In other words, for INLK, the peptide penetrates the membrane with a chain-like structure (Fig. S7b).

It is shown that the arginine and lysine residues in cell-penetrating peptides modulate the penetration process through the electrostatic interactions with the phosphate groups in phospholipids molecules[3]. Our simulation results show that the adhesion of the peptides is partly because of the electrostatic attraction between the negative charges on the phosphate groups of lipid molecules and the positive charges on the side chains of the peptides. Besides, Fig. S7c indicates that there exist hydrogen bonds between these lysine residues and the phospholipid head groups. Further analysis suggests that the main contribution to the hydrogen bonds comes from the NH_3^+ on the side chains of the lysine residues and the PO_4^- of the phosphate groups. As shown in the figure, a side chain of the lysine residue forms at least one and at most three hydrogen bonds with the phosphate groups. This is in line with the results obtained by Lee et al.[4] that the lysine residues play an important role in the interactions between Tp10 and POPC membrane.

Note 2: Water pore formation at a high transmembrane potential in the absence of CPPs

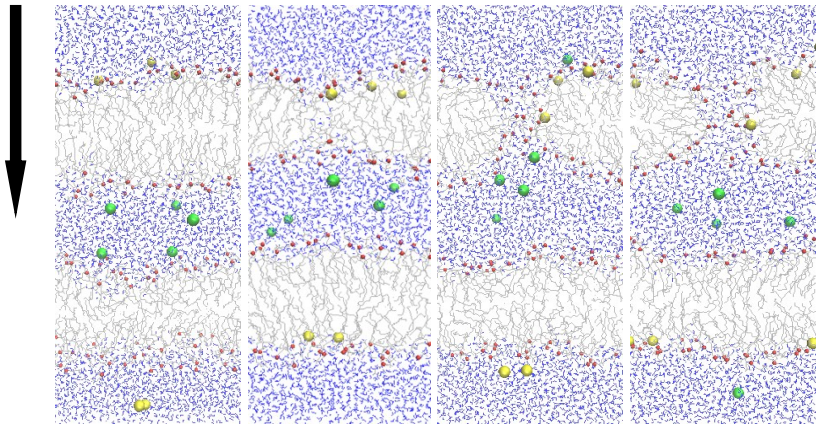

Fig. S8 Snapshots for pore formation in the two-bilayer system with five sodiums (yellow) in the extracellular region and five chlorines (green) in the intracellular region. The water molecules are colored in blue. The lipids are in gray, and in order to show the formation of hydrophilic pore, the phosphate groups are displayed with red beads.

When CPPs is absent, the processes of water pore formation in the presence of ionic imbalance were also investigated here. As demonstrated by other authors[1, 2], we confirmed that in the absence of CPPs, the ionic imbalance may lead to the formation of water pores on the membrane (see Fig. S8). Our simulations indicate that if the transmembrane potential induced by the ionic imbalance is sufficiently high, membrane is deformed and the positions of the phospholipid phosphate groups show a strong fluctuation along z axis, which induces several water molecules aligning their dipoles and stretching inside the hydrophobic part of the bilayer. With a single line of water molecules passing across the membrane, the chain of water molecules may gradually expand into a cylindrical water pore (Fig. S8). After the formation of membrane pores, Cl^- ions will cross the membrane hole that induces a decrease of the membrane potential, and as a result the membrane hole gradually approaches closure. For Na^+ ions, however, they tend to adhere to the membrane, and therefore less crossing events are observed due to their reduced mobility.

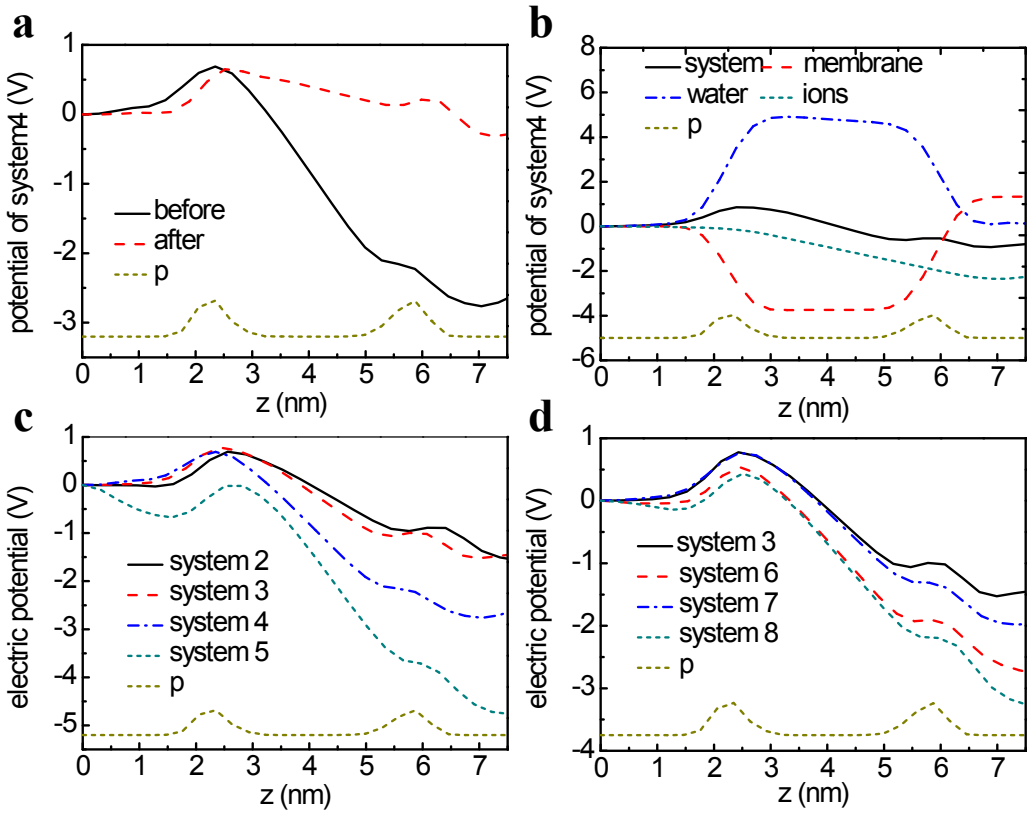

Fig. S9 Electric potential along the z axis for half of the simulation box. For each z position, the charge density was calculated over all charges at the corresponding xy plane. (a) Electric potential before and after the pore formation for the system having five pairs of ionic imbalance (system 4). (b) Contribution of each component to the production of the electric potential in the system. Electric potential for different systems characterized with (c) different pairs of ionic imbalance and (d) different ion concentrations. The potential was calculated with Poisson's equation by integrating twice of the charge distribution ρ(z) along the z- axis. The protrusions in the brown dashed line denoted with p indicate the average position of phosphorus atoms of lipids.

Our simulations (systems 1-5) show that in the absence of CPPs, the membrane hole formation was observed only for the cases having at least a net charge difference of five pairs, below which the membrane would remain integrity within the simulation time we covered (see Table 1). For the system with five pair of ionic imbalance, the electric potential profiles before and after creating a pore are showed in Fig. S9a. Various contributions from different components toward the membrane potential are

shown in Fig. S8b, indicating the dominating contribution of the ionic imbalance on the membrane potential. For example, as shown in systems 2-5, increasing the net charge difference usually results in a higher membrane potential (see Fig. S9c). This observation can interpret our simulation observations for a variety of situations that increasing the net charge difference would promote the pore formation (see Table 1). For the same reason, a significant decrease of membrane potential after the pore formation is caused by transporting ions across the formed pore. In contrast, adding the same number of positive and negative ions to both sides corresponds to the increase of salt concentration (systems 6-8 and systems 9-10), inducing a much weaker effect on membrane potential (Fig. S9d).

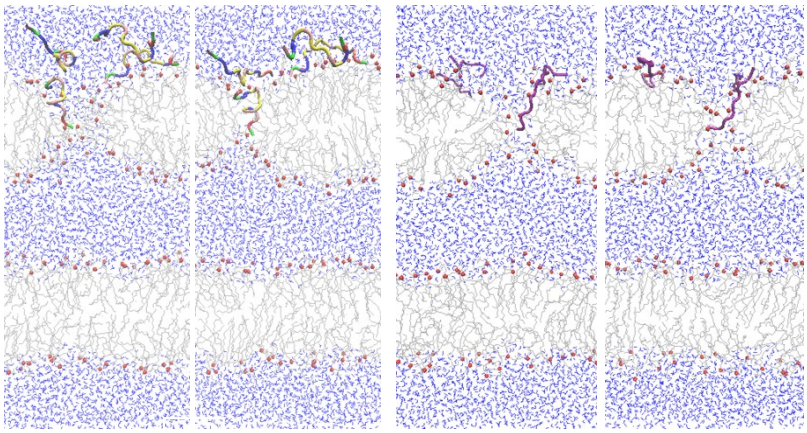

Fig. S10 The configurations at 100ns (left) and 300ns (right) for different peptides. (a) INLK and (b) R9 under a membrane potential corresponding to a net charge difference of five pairs.

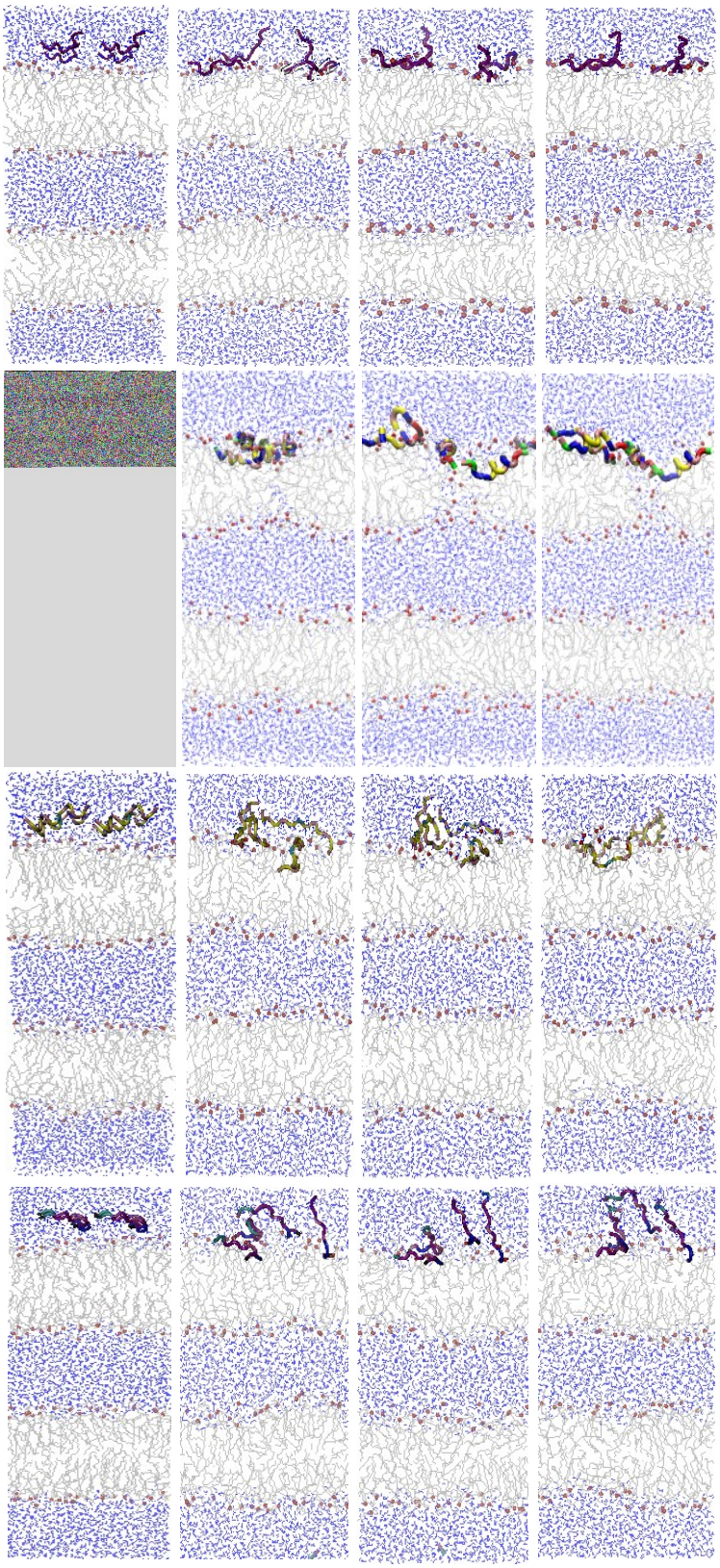

Fig. S11 Time sequences of typical snapshots depicting interactions of different peptides, including R9, ILNK, WALP and TAT, with the DPPC membrane in the presence of membrane potential induced by three pairs of ionic imbalance.

References

1. Gurtovenko, A.A. & Vattulainen, I. Pore Formation Coupled to Ion Transport through Lipid Membranes as Induced by Transmembrane Ionic Charge Imbalance: Atomistic Molecular Dynamics Study. *J. Am. Chem. Soc.* **127**, 17570-17571 (2005).
2. Kandasamy, S.K. & Larson, R.G. Cation and anion transport through hydrophilic pores in lipid bilayers. *J. Chem. Phys.* **125**, 074901-074901 (2006).
3. Herce, H.D., Garcia, A.E. & Cardoso, M.C. Fundamental molecular mechanism for the cellular uptake of guanidinium-rich molecules. *J. Am. Chem. Soc.* **136**, 17459 (2014).
4. Dunkin, C.M. Molecular Dynamics Studies of Transportan 10 (Tp10) Interacting with a POPC Lipid Bilayer. *J. Phys. Chem. B* **115**, 1188-1198 (2011).